



HAL
open science

Structural insight into metallocofactor maturation in carbon monoxide dehydrogenase

Elizabeth Wittenborn, Steven E Cohen, Meriem Merrouch, Christophe Léger, Vincent Fourmond, Sébastien Dementin, Catherine Drennan

► **To cite this version:**

Elizabeth Wittenborn, Steven E Cohen, Meriem Merrouch, Christophe Léger, Vincent Fourmond, et al.. Structural insight into metallocofactor maturation in carbon monoxide dehydrogenase. *Journal of Biological Chemistry*, In press, pp.jbc.RA119.009610. 10.1074/jbc.RA119.009610 . hal-02188452

HAL Id: hal-02188452

<https://amu.hal.science/hal-02188452>

Submitted on 18 Jul 2019

HAL is a multi-disciplinary open access archive for the deposit and dissemination of scientific research documents, whether they are published or not. The documents may come from teaching and research institutions in France or abroad, or from public or private research centers.

L'archive ouverte pluridisciplinaire **HAL**, est destinée au dépôt et à la diffusion de documents scientifiques de niveau recherche, publiés ou non, émanant des établissements d'enseignement et de recherche français ou étrangers, des laboratoires publics ou privés.

Structural insight into metallocofactor maturation in carbon monoxide dehydrogenase

This is the author version of doi:10.1074/jbc.RA119.009610

Elizabeth C. Wittenborn^{1§}, Steven E. Cohen¹, Mériem Merrouch², Christophe Léger², Vincent Fourmond², Sébastien Dementin^{2*}, & Catherine L. Drennan^{1,3,4,5*}

Departments of ¹Chemistry and ³Biology and ⁴Howard Hughes Medical Institute, Massachusetts Institute of Technology, Cambridge, MA 02139, USA

²CNRS, Aix-Marseille Université, Laboratoire de Bioénergétique et Ingénierie des Protéines, Institut de Microbiologie de la Méditerranée, Marseille, France

⁵Fellow, Bio-inspired Solar Energy Program, Canadian Institute for Advanced Research (CIFAR), Toronto, ON M5G 1M1

Running title: *Crystallographic studies of C-cluster assembly*

[§]Current address: California Institute for Quantitative Biosciences, University of California, Berkeley, CA 94720, USA

*To whom correspondence may be addressed:

Catherine L. Drennan, Departments of Chemistry and Biology and Howard Hughes Medical Institute, Massachusetts Institute of Technology, 77 Massachusetts Ave., Cambridge, MA 02139.

Tel.: 617-253-5622; E-mail: cdrennan@mit.edu

Sébastien Dementin, CNRS, Aix-Marseille Université, Laboratoire de Bioénergétique et Ingénierie des Protéines, Institut de Microbiologie de la Méditerranée, Marseille, France.

Tel.: +33 4 91 16 45 29; E-mail: dementin@imm.cnrs.fr

Key words: nickel, iron-sulfur protein, metalloenzyme, one-carbon metabolism, oxidation-reduction (redox), X-ray crystallography, carbon monoxide dehydrogenase (CODH), bioremediation catalyst, heterometallic cofactor

Abstract

The nickel-dependent carbon monoxide dehydrogenase (CODH) employs a unique heterometallic Ni-Fe-S cluster, termed the C-cluster, to catalyze the interconversion of CO and CO₂. Like other complex metalloenzymes, CODH requires dedicated assembly machinery to form the fully intact and functional C-cluster. In particular, nickel incorporation into the C-cluster depends on the maturation factor CooC; however, the mechanism of nickel insertion remains poorly understood. Here, we compare X-ray structures (1.50–2.48 Å resolution) of CODH from *Desulfovibrio vulgaris* (*Dv*CODH) heterologously expressed in either the absence (*Dv*CODH^{-CooC}) or presence (*Dv*CODH^{+CooC}) of co-expressed CooC. We find that the C-cluster of *Dv*CODH^{-CooC} is fully loaded with iron but does not contain any nickel. Interestingly, the so-called unique iron ion

(Fe_u) occupies both its canonical site (80% occupancy) and the nickel site (20% occupancy), with addition of reductant causing further mismetallation of the nickel site (60% iron occupancy). We also demonstrate that a *Dv*CODH variant that lacks a surface-accessible Fe-S cluster (the D-cluster) has a C-cluster that is also replete in iron but lacks nickel, despite co-expression with CooC. In this variant, all Fe_u is in its canonical location and the nickel site is empty. This D-cluster-deficient CODH is inactive despite attempts to reconstitute it with nickel. Taken together, these results suggest that an empty nickel site is not sufficient for nickel incorporation. Based on our findings, we propose a model for C-cluster assembly that requires both CooC and a functioning D-cluster, involves precise redox-state control, and includes a two-step nickel-binding process.

Introduction

Anaerobic carbon monoxide dehydrogenases (CODHs) catalyze the reversible oxidation of CO to CO₂, enabling certain microbes, such as *Rhodospirillum rubrum* and *Carboxydotherrmus hydrogenoformans*, to live on CO as a sole source of carbon and energy (1,2). This microbial activity accounts for the removal of an estimated 10⁸ tons of CO from the lower atmosphere each year, making CODHs an important part of the global carbon cycle (3). Given that CO is a toxic pollutant and a component of fossil fuel emissions, CODH has attracted attention as a possible bioremediation catalyst. Similarly, CODHs also have potential applications in the capture and removal of CO₂ via the Wood-Ljungdahl pathway of carbon fixation, in which the CO that is generated is incorporated into the acetyl group of acetyl-CoA (4). Use of CODH in such capacities would benefit from an ability to produce large amounts of active enzyme. In particular, CODH activity requires a complex heterometallic Ni-Fe-S cofactor (termed the C-cluster), the biogenesis of which is poorly understood.

The CODH C-cluster is housed within a homodimeric protein scaffold that contains two additional Fe-S clusters, termed the B- and D-clusters, that are used for electron transfer during catalysis (Figure 1A). The D-cluster, depending on the bacterial species, is either a [4Fe-4S] or [2Fe-2S] cluster that resides at the CODH dimer interface and serves as an electron conduit to external redox partners, such as ferredoxins; whereas the B-cluster is a [4Fe-4S] cluster that mediates electron transfer between the C- and D-clusters (5-9). The C-cluster is a structurally unique metallocluster composed of a distorted [Ni-3Fe-4S] cubane linked through a sulfide ion (S_L) to a mononuclear iron site (Fe_u) (Figure 1B) (5,6). This canonical C-cluster architecture is essential for catalysis, as it allows for binding of CO at the nickel ion of the cubane, activating it for nucleophilic attack by a water molecule ligated in immediate proximity at Fe_u (10-13). To access this chemistry, organisms require dedicated cellular machinery for C-cluster assembly, similar to the requirements of other complex metalloclusters (14). Our understanding of the C-cluster assembly process, however, remains incomplete. It is still unknown what the biosynthetic origin of the Fe-S scaffold of the cluster is, how the Ni-Fe-S cluster

is assembled, and what roles individual accessory proteins play in this assembly process.

Limited insight into the process of C-cluster assembly has been gleaned from the co-operonic expression of accessory proteins that appear to play roles in cluster maturation, in particular incorporation of nickel. Previous studies have shown that integration of nickel into the C-cluster is dependent on the accessory protein CooC (15-17). Certain organisms express additional proteins, CooJ and CooT, that have been implicated in C-cluster maturation; however, CooC appears to be the only dedicated and essential maturation factor expressed by all CODH-containing organisms (15,18-22). CooC is a P-loop ATPase with sequence similarity to UreG and HypB, maturation factors involved in nickel transfer to the active sites of urease and Ni-Fe hydrogenase, respectively (15,23). In analogy to UreG and HypB, CooC has been proposed to use ATP hydrolysis to facilitate nickel insertion into CODH (15,16,23,24). Alternatively, CooC has been proposed to fold or otherwise mediate formation of the proper nickel binding site in CODH (16,17,25).

To gain a further understanding of C-cluster maturation and the role of CooC, we have recently developed a means to heterologously express *Desulfovibrio vulgaris* CODH (*Dv*CODH) in either the presence (*Dv*CODH^{+CooC}) or absence (*Dv*CODH^{-CooC}) of the *D. vulgaris* CooC maturase (*Dv*CooC) using *D. fructosovorans* as an expression host (17). This differential expression results in substantially different enzymatic phenotypes (Table 1). As-isolated *Dv*CODH^{+CooC} binds about half of the expected nickel content and exhibits a lag phase in activity followed by a relatively low rate of CO oxidation (160 μmol·min⁻¹·mg⁻¹) as compared to the previously published activities of monofunctional CODHs from other species, which range from ~4400–16,000 μmol·min⁻¹·mg⁻¹ (17,26,27). Incubation of the as-isolated *Dv*CODH^{+CooC} with both NiCl₂ and the reductant sodium dithionite results in elimination of the lag phase and a 10-fold increase in CO oxidation activity; however, activation does not occur in the presence of NiCl₂ or sodium dithionite alone (17). In contrast, as-isolated *Dv*CODH^{-CooC} contains low amounts of nickel (0–0.2 Ni/monomer), has nearly no activity (4% of as-isolated *Dv*CODH^{+CooC}), and undergoes limited

activation with NiCl₂ and sodium dithionite (17), suggesting that DvCooC is involved in constructing the appropriate nickel binding site in DvCODH (25).

Interestingly, our previously published crystal structures of DvCODH^{+CooC} revealed that the C-cluster adopts an alternative conformation upon exposure to oxygen in which the Ni, Fe_u, and S_L ions shift by as much as 3 Å and the Ni and Fe_u ions adopt new coordination environments (Figure 1C) (9). Notably, this oxidized conformation of the C-cluster can be converted back to the canonical, reduced conformation by incubation with reducing agent (9). The oxidized conformation involves ligation by a cysteine residue that is strictly conserved in CODHs but that does not serve as a ligand to the active, reduced conformation of the cluster (9). Mutation of this cysteine residue (Cys 301) in DvCODH^{+CooC} to serine (C301S) was shown to result in inactive enzyme that does not bind nickel (Table 1) (9), similar to previous results on the CODH from *Moorella thermoacetica* (28). The crystal structure of DvCODH(C301S)^{+CooC} revealed a partially assembled C-cluster in which Fe_u adopted a split conformation: at 70% occupancy Fe_u was in its canonical binding site; and at 30% occupancy Fe_u was incorporated into the cubane portion of the cluster, taking up the canonical Ni binding site (Figure 1D) (9). This split C-cluster conformation combined with the inability of the DvCODH(C301S)^{+CooC} variant to incorporate nickel led us to propose that the oxidized conformation of the cluster could be an intermediate in C-cluster maturation, although how this conformation may participate in the assembly process remained unclear (9).

To further interrogate the process of C-cluster assembly, we have now determined crystal structures of DvCODH produced in the absence of CooC (DvCODH^{-CooC}) and of a DvCODH variant produced in the presence of CooC and engineered to not contain the surface-accessible D-cluster (DvCODH(ΔD)^{+CooC}). Comparison of the DvCODH^{-CooC} structure to that of DvCODH(C301S)^{+CooC} (9) suggests a possible link between CooC-dependent cluster assembly and the ability to adopt the alternative, oxidized cluster arrangement. Furthermore, removal of the D-cluster leads to formation of an incomplete C-cluster, highlighting the importance of this

redox active iron-sulfur cluster for C-cluster maturation. Combined, these results expand our understanding of C-cluster biogenesis, with an emphasis on the importance of accessing different cluster conformations and redox states.

Results

The C-cluster expressed in the absence of CooC is a [3Fe-4S] cluster with a mobile fourth iron. The CODH from *D. vulgaris* was expressed heterologously in *D. fructosovorans* in the absence of the C-cluster maturation factor CooC (DvCODH^{-CooC}), as described previously (17). The preparation of protein that was used for crystallization displayed no detectible CO oxidation activity and contained 0 Ni/monomer and 10 Fe/monomer (Table 1). The crystal structure of DvCODH^{-CooC} was determined to 1.50-Å resolution (Table 2). The structure aligns well (Cα r.m.s.d. of 0.18 Å for 1250 Cα atoms within the CODH dimer) with our previously determined structure of DvCODH^{+CooC} (9) and the B- and D-clusters of the enzyme are both present and fully intact. Thus, the overall structure of DvCODH is retained when expressed in the absence of CooC.

At the C-cluster of DvCODH^{-CooC}, the [3Fe-4S] partial cubane portion of the canonical C-cluster is intact and present at full occupancy (Figure 2), indicating that CooC is not necessary for formation of this part of the C-cluster. Modeling of the Fe_u ion, however, was more complicated. When the C-cluster was modeled as a [3Fe-4S]-Fe_u cluster at full occupancy, residual positive difference electron density was observed in the open cubane position, indicating the presence of an additional atom (Figure 2A). Further, iron anomalous difference maps (Table 2) reveal a shoulder extending from the canonical Fe_u binding site into the cubane position, suggesting the presence of iron at partial occupancy (Figure 2B). Given the lack of nickel in the sample that was crystallized, the positive difference density in the electron density maps, and the shoulder in the iron anomalous maps, we rationalized that Fe_u could be present in a split conformation. Refinement of Fe_u with a split conformation revealed that at 80% occupancy Fe_u is in its canonical binding site, ligated by His 266, Cys 302, and a water molecule; whereas at 20% occupancy, Fe_u is incorporated into the cubane

portion of the cluster and ligated by Cys 519, forming a distorted [4Fe-4S] cluster (Figure 2C). Similar split Fe_u conformations were observed across multiple crystal structures of $DvCODH^{-CooC}$ samples that lacked nickel. Interestingly, this split Fe_u conformation is similar to what was observed previously in our structure of $DvCODH(C301S)^{+CooC}$ (9) (see Figure 1D), a CODH variant that is unable to adopt the alternative, oxidized C-cluster conformation due to the absence of the Cys 301 thiol for coordination to Fe_u . Together, the structural similarity between the C-clusters in $DvCODH^{-CooC}$ and $DvCODH(C301S)^{+CooC}$ (9) suggest a link between Cys 301 and the role of CooC in cluster assembly, perhaps due to a CooC-induced conformational change in which Fe_u becomes ligated by Cys 301 (see Discussion). Additionally, these data suggest that it is not the lack of an open coordination site for nickel that prevents nickel incorporation into the C-cluster. Although there is some Fe_u in the Ni binding site, there is not enough to explain the inability to reconstitute the C-cluster with nickel.

Reduction of $DvCODH^{-CooC}$ induces movement of Fe_u into the cubane position. The presence of Fe_u at partial occupancy in the Ni binding site of the C-cluster in both our new structure, $DvCODH^{-CooC}$, and previous structure, $DvCODH(C301S)^{+CooC}$ (9), is intriguing. Notably, the [3Fe-4S] clusters of aconitase and ferredoxins, as well as synthetic model compounds, are well known to incorporate exogenous metal into their open cubane site upon reduction due to the increased nucleophilicity of the open sulfide ions in the reduced state (29-33). Therefore, we hypothesized that reduction of the immature pre-C-cluster, which in part resembles a [3Fe-4S] cluster, could have led to movement of Fe_u from its canonical binding site into the cubane position in some CODH molecules. To test this hypothesis, crystals of as-isolated $DvCODH^{-CooC}$ were soaked in the reductant sodium dithionite prior to cryo-cooling and X-ray data collection. The structure of reduced $DvCODH^{-CooC}$ was determined to 1.72-Å resolution (Table 2) and reveals greater incorporation of Fe_u into the cubane position relative to the structure of the as-isolated enzyme (Figure 3A,B). Here, the Fe_u ion resides in its canonical position at 40% occupancy and in the cubane portion at 60% occupancy (Figure 3C).

Together, these data suggest that reduction of the pre-C-cluster before Ni is inserted can lead to mismetallation of the Ni site, and therefore careful control of cluster redox state is likely essential during the C-cluster maturation process *in vivo*.

The D-cluster is necessary for proper C-cluster assembly in the presence of CooC. To test the hypothesis that control of redox state is essential to C-cluster maturation, we sought to disrupt electron transfer between the C-cluster and external redox partners by removal of the solvent-exposed D-cluster, which serves as an electron conduit during CO/CO₂ interconversion. Towards this goal, we designed a $DvCODH$ double-mutant variant in which the D-cluster-ligating cysteine residues (Cys 42 and Cys 45) were replaced with alanine residues to abolish binding of the D-cluster ($DvCODH(\Delta D)$). This variant was expressed in the presence of CooC ($DvCODH(\Delta D)^{+CooC}$) and purified to homogeneity. Similar to $DvCODH^{-CooC}$ and $DvCODH(C301S)^{+CooC}$, $DvCODH(\Delta D)^{+CooC}$ is inactive as-isolated and does not contain appreciable amounts of Ni (Table 1). No increase in activity is observed upon incubation with nickel (Table 1). These observations indicate that the D-cluster is essential for C-cluster maturation.

To characterize the impact of a D-cluster deletion on C-cluster architecture, the crystal structure of $DvCODH(\Delta D)^{+CooC}$ was determined to 2.48-Å resolution (Table 2). The overall structure aligns well (Ca r.m.s.d of 0.29 Å for 1242 Ca atoms within the CODH dimer) with that of $DvCODH^{+CooC}$. The structure contains both the B- and C-clusters and confirms that the D-cluster is not present in this protein variant (Figure 4A). The absence of the D-cluster leads to local disorder, and residues 41–44 could not be modeled (Figure 4A inset). At the C-cluster of $DvCODH(\Delta D)^{+CooC}$, we observe an intact [3Fe-4S]- Fe_u scaffold with Fe_u present at 100% occupancy in its canonical binding site (Figure 4B,C). This result is consistent with the above-mentioned idea that movement of Fe_u into the cubane is induced by reduction and that the D-cluster mediates that reduction. Additionally, it is notable that the C-cluster of $DvCODH(\Delta D)^{+CooC}$, in which 100% of Fe_u is in the canonical location, cannot be activated by incubation with nickel. Further, the fact that the structure of $DvCODH(\Delta D)^{+CooC}$ is largely unchanged by D-cluster loss suggests that

it is the D-cluster's redox role, rather than a structural role, that is required for nickel insertion.

Discussion

Here we present a series of crystal structures of DvCODH to provide insight into the process of C-cluster assembly and maturation, the mechanisms of which remained largely elusive. Our structures suggest that the C-cluster maturase CooC is primarily involved in nickel insertion rather than in formation of the [3Fe-4S]-Fe_u scaffold and reveal that nickel insertion is additionally dependent on the D-cluster, likely due to its role in mediating electron transfer. Together, these findings allow us to propose a model for C-cluster assembly and maturation involving multiple cluster conformations and redox states.

In our structure of as-isolated DvCODH^{-CooC}, we observe a largely (80%) intact Fe-S scaffold that contains 4 Fe ions and 4 S ions arranged as a [3Fe-4S]-Fe_u "pre-C-cluster" that lacks nickel. The presence of this prearranged Fe-S scaffold in the absence of dedicated C-cluster assembly machinery suggests that the [3Fe-4S]-Fe_u cluster arrangement can be formed using general Fe-S cluster biogenesis pathways, such as the SUF or NIF systems, both of which are present in the *D. fructosovorans* expression host as well as *D. vulgaris* itself. Two possibilities for the formation of the Fe-S scaffold can be envisioned (Figure 5A). First, the pre-C-cluster could be inserted in two pieces: a single iron ion inserted into the unique His 266/Cys 302 site and a [3Fe-4S] cluster inserted into the cubane site. Linkage of Fe_u and the [3Fe-4S] cluster via the cubane sulfide (S_L) could occur subsequently (Figure 5A, upper pathway). Alternatively, the C-cluster binding site of CODH could become loaded with a [4Fe-4S] cluster that is distorted by CODH concomitant with the insertion step or is acted upon by an unknown maturation factor to remove an iron ion from the cubane, forming Fe_u (Figure 5A, lower pathway). Regardless of the exact assembly mechanism, our data indicate that CooC is not necessary for formation of a 4-Fe containing Fe-S scaffold and that its primary role is likely in facilitating nickel insertion.

Once the Fe-S framework of the C-cluster has been assembled in CODH, nickel insertion can occur to form the fully mature and active cluster. Here we consider two possibilities for nickel

insertion. In the first, C-cluster maturation *in vivo* involves the CooC-dependent insertion of nickel into a preformed [3Fe-4S]-Fe_u scaffold that resembles our DvCODH^{-CooC} structures with Fe_u in its canonical site coordinated by His 266 and Cys 302 (Figure 5B). In the second, nickel is inserted into a [3Fe-4S]-Fe_u scaffold in which Cys 301 coordinates Fe_u (Figure 5C), a state that is reminiscent of the metal positions observed in our previous structure of fully oxidized DvCODH^{+CooC} (Figure 1C) (9).

For scenario I (Figure 5B), the key role of CooC, in addition to nickel insertion, may be to control the redox state of the pre-C-cluster, allowing for nickel insertion without mismetallation of the nickel site. In analogy to metal capture by [3Fe-4S] clusters in other systems, nickel insertion into the scaffold as shown in Figure 5B would likely require that the [3Fe-4S] framework be in a reduced state to increase the nucleophilicity of the open cubane site, allowing for binding of exogenous metal (29-33). In the case of the C-cluster, however, addition of exogenous nickel is likely complicated by the presence of Fe_u, which we have shown can migrate into the open coordination site of the reduced cubane (Figures 2, 3). In the context of C-cluster assembly, this observation indicates that the redox state of the pre-C-cluster must be tightly regulated to avoid mismetallation. One strategy for ensuring Ni incorporation *in vivo* could be to couple binding of CooC with cluster reduction, such that cluster reduction occurs just prior to nickel insertion. For example, binding of CooC could in some way facilitate interaction of CODH with a low-potential electron transfer protein, such as a reduced ferredoxin.

Although control of cluster reduction provides one route to prevent mismetallation, the previously reported structure of a fully oxidized C-cluster (Figure 1C)(9) suggests another possible strategy for avoiding incorporation of Fe_u into the cubane *in vivo* (Figure 5C). In particular, the position of Fe_u in the oxidized cluster, ligated by Cys 301, could represent an alternative binding site in which Fe_u is positioned prior to nickel insertion, such that Fe_u is not ligated in immediate proximity to the remainder of the [3Fe-4S] scaffold (Figure 5C, state II). In this model, CooC could be involved in inducing a conformational change in the C-cluster prior to nickel insertion such that Fe_u

becomes ligated by Cys 301 (Figure 5C, state I to II). Given the inability of the C-cluster to incorporate nickel in the absence of the D-cluster, this conformational change could additionally be redox-dependent. In any case, nickel could then be inserted into the His 266/Cys 302 binding site that is normally occupied by Fe_u, resulting in formation of the oxidized C-cluster conformation (Figure 5C, state IIIa). Subsequent reduction, possibly facilitated by a change in reduction potential as a result of nickel binding, would then trigger formation of the active C-cluster via the three-atom migration of Fe_u, S_L, and Ni that we have described previously and that occurs upon reduction of the oxidized cluster conformation (Figure 5C, state IIIa to IV) (9).

With these two proposals in mind (Figure 5B and 5C), we revisited the CODH literature. In addition to our previous characterization of *Dv*CODH(C301S)^{+CooC} (9), several additional mutagenesis studies on the CODHs from *Moorella thermoacetica* (*Mt*CODH) (28), *Rhodospirillum rubrum* (*Rr*CODH) (34-36), and *Carboxydotherrmus hydrogenoformans* (*Ch*CODH-II) (37) are better explained by the mechanism shown in Figure 5C than Figure 5B. First, the proposal in Figure 5B does not explain why substitution of the non-canonical C-cluster ligand Cys 301 in *Dv*CODH and *Mt*CODH results in inactive CODH variants that lack nickel (9,28), whereas the mechanism in Figure 5C provides a role for Cys 301 in nickel insertion. Second, substitution of the C-cluster-ligating histidine residue with valine (in *Rr*CODH) or alanine (in *Ch*CODH-II) resulted in CODHs with iron contents that were indistinguishable from wild-type, but that were impaired in their ability to incorporate nickel *in vivo* (34,37). Additional mutagenesis experiments in which each of the canonical C-cluster-ligating cysteine residues were mutated to alanine or serine, revealed that His 266 and Cys 302 (*D. vulgaris* numbering) are in fact the only protein-based ligands to the canonical C-cluster that are necessary for nickel incorporation (34-37). Together, these data support the hypothesis that the His 266/Cys 302 site serves as the binding site for nickel during nickel incorporation (Figure 5C). Second, the kinetics of nickel activation in nickel-deficient *Rr*CODH (produced in the presence of *Rr*CooC) suggest a two-step mechanism in which nickel

first binds to the enzyme reversibly and then is seated into its active and stable site (26,36).

Collectively, these findings support a model in which Cys 301 binds Fe_u while nickel is first inserted into the His 266/Cys 302 site, followed by rearrangement to form the active C-cluster (Figure 5C, upper pathway), consistent with structures of the C-cluster that we have observed experimentally (9). We note that an alternative assembly pathway could also involve coordination of Fe_u by Cys 301 while nickel is inserted into its canonical site in the Fe-S cubane, although such a state has not been observed crystallographically (Figure 5C, state IIIb) and does not explain the *Rr*CODH mutational data mentioned above. One caveat of this model is that we have only observed Fe_u coordinated to Cys 301 in the oxidized state of the C-cluster (9), whereas the presence of reducing agent is known to be essential for nickel-dependent activation *in vitro* (17,26). That being said, it has not yet been possible to visualize a nickel-deficient form of *Dv*CODH^{+CooC} in either an oxidized or reduced state to know whether Fe_u movement occurs and/or is redox-dependent in the absence of nickel.

Overall, our data begin to reveal the requirements for assembly of a fully intact and activatable C-cluster: 1) the C-cluster maturase CooC (this work)(15-17), 2) the D-cluster (this work), and 3) the non-canonical Fe_u ligand Cys 301 (9,28). Together, these observations begin to expand our understanding of the complex and tightly-regulated process of C-cluster biogenesis. In particular, given the varied metal binding sites that we have observed within the C-cluster scaffold, the insertion of nickel is not a straightforward process and appears to be more complicated than originally thought.

Experimental Procedures

Cloning and purification of DvCODH^{-CooC} and DvCODH(ΔD)^{+CooC}. Protein was expressed and purified as described previously (17). Briefly, the *D. vulgaris* gene encoding CODH (*cooS*) was cloned into a modified pBGF4 shuttle vector under the control of the promoter of the *D. fructosovorans* Ni-Fe hydrogenase operon and included an N-terminal strep-tag. For *Dv*CODH(ΔD)^{+CooC}, the expression vector also contained the gene for the CooC maturase (*cooC*), and mutations encoding C42A and C45A were

introduced into the *cooS* gene by site-directed mutagenesis. To perform mutagenesis by PCR, the HindIII-SacI fragment of the modified pBGF4 plasmid, containing the 5' end of *cooS*, was subcloned into pUC19 to serve as a DNA template. The primers GAACAGACGCCGCGCCAA ATTCGCGAATTGGGCACCACC (forward; mutations underlined) and GGTGGTGCCCA ATTCGCGAATTTGGCGCGCGTCTGTT C (reverse; mutations underlined) were used to generate the C42A/C45A variant. The mutated HindIII-SacI fragment was then reintroduced into the HindIII-SacI digested expression vector. The final mutated plasmid was verified by DNA sequencing. Protein was expressed in *D. fructosovorans* and purified under strictly anaerobic conditions in a Jacomex anaerobic chamber (100% N₂ atmosphere) by affinity chromatography on Strep-Tactin Superflow resin. Protein concentrations were determined by amino acid analysis at the Centre for Integrated Structural Biology (Grenoble, France). Metal content was analyzed by inductively coupled plasma optical emission spectroscopy (ICP-OES). The as-isolated samples contained Ni and Fe as follows: *DvCODH*^{-CooC}: 0 Ni/monomer, 10 Fe/monomer; *DvCODH*(Δ)^{+CooC}: 0.02 Ni/monomer, 8.5 Fe/monomer. CO oxidation activity was assayed at 37 °C by monitoring the reduction of methyl viologen at 604 nm ($\epsilon = 13.6 \text{ mM}^{-1}\cdot\text{cm}^{-1}$), as described previously (17). Neither *DvCODH*^{-CooC} nor *DvCODH*(Δ)^{+CooC} exhibited detectable CO oxidation activity. Reconstitution of either sample with NiCl₂ under reducing conditions did not lead to an increase in activity.

Crystallization of DvCODH variants. *DvCODH*^{-CooC} and *DvCODH*(Δ)^{+CooC} were crystallized in an N₂ atmosphere at 21 °C by hanging drop vapor diffusion in an MBraun anaerobic chamber. A 1- μ L aliquot of protein (10 mg/mL in 100 mM Tris-HCl pH 8) was combined with 1 μ L of a precipitant solution (200–275 mM MgCl₂, 14–20% PEG 3350) on a glass cover slip and sealed over a reservoir containing 500–700 μ L of precipitant solution. Diffraction quality crystals grew in 4–7 days. Crystals were soaked in a cryo-protectant solution containing 200 mM MgCl₂, 20–30% PEG 3350, and 10–16% glycerol and cryo-cooled in liquid nitrogen. For structures of reduced *DvCODH*^{-CooC},

crystals were soaked in 250 mM MgCl₂, 18% (w/v) PEG 3350, 5 mM sodium dithionite for 30 min prior to cryo-protecting and cryo-cooling in liquid nitrogen.

Data collection, model building, and refinement. Data were collected at the Advanced Photon Source (Argonne, IL) on beamline 24-ID-C using a Pilatus 6M pixel detector and at a temperature of 100 K. Native and Fe peak data were collected on the same crystal for each sample, where applicable. The *DvCODH*(Δ)^{+CooC} structure was determined and refined using data collected at the Fe peak wavelength. Data for *DvCODH*^{-CooC} (as-isolated and reduced) were integrated in XDS and scaled in XSCALE (38). Data for *DvCODH*(Δ)^{+CooC} were integrated and scaled in HKL2000 (39). All data collection statistics are summarized in Table 2.

Structures were determined by molecular replacement (MR) in the program Phaser (40) using our previously published structure of *DvCODH* (PDB ID: 6B6V) as a search model. Following MR, 10 cycles of simulated annealing refinement were performed in Phenix (41) to eliminate existing model bias. Refinement of atomic coordinates and atomic displacement parameters (*B*-factors) was performed in Phenix and models were completed by iterative rounds of model building in Coot (42) and refinement in Phenix. Metal cluster geometries were restrained during refinement using custom parameter files. In advanced stages of refinement, water molecules were added automatically in Phenix (41) and modified in Coot (42) with placement of additional water molecules until their number was stable. For the *DvCODH*^{-CooC} structures, final stages of refinement included translation, libration, screw (TLS) parameterization with one TLS group per monomer (43). Side chains without visible electron density were truncated to the last atom with electron density and amino acids without visible electron density were not included in the model. Final models contain the following residues (of 629 total): as-isolated *DvCODH*^{-CooC}: 4–628 (chain A), 4–629 (chain B), 4–629 (chain C), 3–628 (chain D); reduced *DvCODH*^{-CooC}: 4–629 (chain A), 4–629 (chain B), 4–629 (chain C), 3–629 (chain D); *DvCODH*(Δ)^{+CooC}: 4–40, 45–628 (chain A).

Final refinement yielded models with low free *R*-factors, excellent stereochemistry, and small root mean square deviations from ideal values for bond lengths and angles. Models were validated using simulated annealing composite omit maps calculated in Phenix (41). Model geometry was analyzed using MolProbity (44). Analysis of Ramachandran statistics indicated that each structure contained the following percentages of

residues in the favored, allowed, and disallowed regions, respectively: as-isolated *DvCODH*^{-CooC}: 96.7%, 3.0%, 0.3%; reduced *DvCODH*^{-CooC}: 96.9%, 2.8%, 0.3%; *DvCODH*(Δ)^{+CooC}: 95.8%, 4.0%, 0.2%. Refinement and geometry statistics are summarized in Table 2. Figures were generated in PyMOL (45). Crystallography packages were compiled by SBGrid (46).

Acknowledgements

The authors thank Marco Jost and David Born for helpful conversations and critical reading of the manuscript. This work was supported by National Institutes of Health[§] (NIH) grants T32 GM008334 (ECW and SEC) and R01 GM069857 and R35 GM126982 (CLD); and ANR projects MeCO2Bio and SHIELDS. CLD is a Howard Hughes Medical Institute Investigator and a fellow of the Bio-inspired Solar Energy Program, Canadian Institute for Advanced Research. This work is based on research conducted at the Advanced Photon Source on the Northeastern Collaborative Access Team beamlines, which are funded by the National Institute of General Medical Sciences from the NIH (P41 GM103403). The Pilatus 6M detector on beamline 24-ID-C is funded by a NIH Office of Research Infrastructure Programs High End Instrumentation grant (S10 RR029205). This research used resources of the Advanced Photon Source, a U.S. Department of Energy (DOE) Office of Science User Facility operated for the DOE Office of Science by Argonne National Laboratory under Contract No. DE-AC02-06CH11357. Atomic coordinates and structure factors have been deposited in the Protein Data Bank (www.rcsb.org) under the following accession codes: 6ONC (*Dv*CODH^{-CooC}, as-isolated), 6OND (*Dv*CODH^{-CooC}, reduced), and 6ONS (*Dv*CODH(Δ)^{+CooC}).

[§]The content is solely the responsibility of the authors and does not necessarily represent the official views of the National Institutes of Health.

Conflict of Interest

The authors declare that they have no conflicts of interest with the contents of this article.

Author Contributions

ECW and SEC performed the crystallographic experiments and analyzed the crystallographic data with CLD. MM and SD purified protein and performed activity assays. ECW and CLD wrote the manuscript with critical contributions from CL, VF, and SD.

References

1. Uffen, R. L. (1976) Anaerobic growth of a *Rhodopseudomonas* species in the dark with carbon monoxide as sole carbon and energy substrate. *Proc Natl Acad Sci USA* **73**, 3298-3302
2. Svetlichny, V. A., Sokolova, T. G., Gerhardt, M., Ringpfel, M., Kostrikina, N. A., and Zavarzin, G. A. (1991) *Carboxydotherrmus hydrogenoformans* Gen-Nov, Sp-Nov, a CO-utilizing thermophilic anaerobic bacterium from hydrothermal environments of Kunashir Island. *Syst Appl Microbiol* **14**, 254-260
3. Bartholomew, G. W., and Alexander, M. (1979) Microbial metabolism of carbon monoxide in culture and in soil. *Appl Environ Microbiol* **37**, 932-937
4. Can, M., Armstrong, F. A., and Ragsdale, S. W. (2014) Structure, function, and mechanism of the nickel metalloenzymes, CO dehydrogenase, and acetyl-CoA synthase. *Chem Rev* **114**, 4149-4174
5. Drennan, C. L., Heo, J., Sintchak, M. D., Schreiter, E., and Ludden, P. W. (2001) Life on carbon monoxide: X-ray structure of *Rhodospirillum rubrum* Ni-Fe-S carbon monoxide dehydrogenase. *Proc Natl Acad Sci USA* **98**, 11973-11978
6. Dobbek, H., Svetlitchnyi, V., Gremer, L., Huber, R., and Meyer, O. (2001) Crystal structure of a carbon monoxide dehydrogenase reveals a [Ni-4Fe-5S] cluster. *Science* **293**, 1281-1285
7. Kumar, M., Lu, W. P., Liu, L. F., and Ragsdale, S. W. (1993) Kinetic evidence that carbon monoxide dehydrogenase catalyzes the oxidation of carbon monoxide and the synthesis of acetyl-CoA at separate metal centers. *J Am Chem Soc* **115**, 11646-11647
8. Anderson, M. E., and Lindahl, P. A. (1994) Organization of clusters and internal electron pathways in CO dehydrogenase from *Clostridium thermoaceticum*: relevance to the mechanism of catalysis and cyanide inhibition. *Biochemistry* **33**, 8702-8711
9. Wittenborn, E. C., Merrouch, M., Ueda, C., Fradale, L., Leger, C., Fourmond, V., Pandelia, M. E., Dementin, S., and Drennan, C. L. (2018) Redox-dependent rearrangements of the NiFeS cluster of carbon monoxide dehydrogenase. *Elife* **7**, e39451
10. Hu, Z. G., Spangler, N. J., Anderson, M. E., Xia, J. Q., Ludden, P. W., Lindahl, P. A., and Munch, E. (1996) Nature of the C-cluster in Ni-containing carbon monoxide dehydrogenases. *J Am Chem Soc* **118**, 830-845
11. DeRose, V. J., Telser, J., Anderson, M. E., Lindahl, P. A., and Hoffman, B. M. (1998) A multinuclear ENDOR study of the C-cluster in CO dehydrogenase from *Clostridium thermoaceticum*: Evidence for H_xO and histidine coordination to the [Fe₄S₄] center. *J Am Chem Soc* **120**, 8767-8776
12. Jeung, J. H., and Dobbek, H. (2007) Carbon dioxide activation at the Ni,Fe-cluster of anaerobic carbon monoxide dehydrogenase. *Science* **318**, 1461-1464
13. Kung, Y., Doukov, T. I., Seravalli, J., Ragsdale, S. W., and Drennan, C. L. (2009) Crystallographic snapshots of cyanide- and water-bound C-clusters from bifunctional carbon monoxide dehydrogenase/acetyl-CoA synthase. *Biochemistry* **48**, 7432-7440
14. Shepard, E. M., Boyd, E. S., Broderick, J. B., and Peters, J. W. (2011) Biosynthesis of complex iron-sulfur enzymes. *Curr Opin Chem Biol* **15**, 319-327
15. Kerby, R. L., Ludden, P. W., and Roberts, G. P. (1997) In vivo nickel insertion into the carbon monoxide dehydrogenase of *Rhodospirillum rubrum*: Molecular and physiological characterization of *cooCTJ*. *J Bacteriol* **179**, 2259-2266
16. Jeon, W. B., Cheng, J. J., and Ludden, P. W. (2001) Purification and characterization of membrane-associated CooC protein and its functional role in the insertion of nickel into carbon monoxide dehydrogenase from *Rhodospirillum rubrum*. *J Biol Chem* **276**, 38602-38609
17. Hadj-Saïd, J., Pandelia, M. E., Léger, C., Fourmond, V., and Dementin, S. (2015) The carbon monoxide dehydrogenase from *Desulfovibrio vulgaris*. *Biochim Biophys Acta* **1847**, 1574-1583
18. Watt, R. K., and Ludden, P. W. (1998) The identification, purification, and characterization of CooJ. A nickel-binding protein that is co-regulated with the Ni-containing CO dehydrogenase from *Rhodospirillum rubrum*. *J Biol Chem* **273**, 10019-10025

19. Jeoung, J. H., Goetzl, S., Hennig, S. E., Fessler, J., Wormann, C., Dendra, J., and Dobbek, H. (2014) The extended reductive acetyl-CoA pathway: ATPases in metal cluster maturation and reductive activation. *Biol Chem* **395**, 545-558
20. Timm, J., Brochier-Armanet, C., Perard, J., Zambelli, B., Ollagnier-de-Choudens, S., Ciurli, S., and Cavazza, C. (2017) The CO dehydrogenase accessory protein CooT is a novel nickel-binding protein. *Metallomics* **9**, 575-583
21. Alfano, M., Perard, J., Miras, R., Catty, P., and Cavazza, C. (2018) Biophysical and structural characterization of the putative nickel chaperone CooT from *Carboxydotherrmus hydrogenoformans*. *J Biol Inorg Chem* **23**, 809-817
22. Alfano, M., Perard, J., Carpentier, P., Basset, C., Zambelli, B., Timm, J., Crouzy, S., Ciurli, S., and Cavazza, C. (2019) The carbon monoxide dehydrogenase accessory protein CooJ is a histidine-rich multidomain dimer containing an unexpected Ni(II)-binding site. *J Biol Chem*
23. Jeoung, J. H., Giese, T., Grunwald, M., and Dobbek, H. (2009) CooC1 from *Carboxydotherrmus hydrogenoformans* is a nickel-binding ATPase. *Biochemistry* **48**, 11505-11513
24. Jeoung, J. H., Giese, T., Grunwald, M., and Dobbek, H. (2010) Crystal structure of the ATP-dependent maturation factor of Ni,Fe-containing carbon monoxide dehydrogenases. *J Mol Biol* **396**, 1165-1179
25. Merrouch, M., Benvenuti, M., Lorenzi, M., Leger, C., Fourmond, V., and Dementin, S. (2018) Maturation of the [Ni-4Fe-4S] active site of carbon monoxide dehydrogenases. *J Biol Inorg Chem* **23**, 613-620
26. Ensign, S. A., Campbell, M. J., and Ludden, P. W. (1990) Activation of the nickel-deficient carbon monoxide dehydrogenase from *Rhodospirillum rubrum*: kinetic characterization and reductant requirement. *Biochemistry* **29**, 2162-2168
27. Svetlitchnyi, V., Peschel, C., Acker, G., and Meyer, O. (2001) Two membrane-associated NiFeS-carbon monoxide dehydrogenases from the anaerobic carbon-monoxide-utilizing eubacterium *Carboxydotherrmus hydrogenoformans*. *J Bacteriol* **183**, 5134-5144
28. Kim, E. J., Feng, J., Bramlett, M. R., and Lindahl, P. A. (2004) Evidence for a proton transfer network and a required persulfide-bond-forming cysteine residue in Ni-containing carbon monoxide dehydrogenases. *Biochemistry* **43**, 5728-5734
29. Zhou, J., Raebiger, J. W., Crawford, C. A., and Holm, R. H. (1997) Metal ion incorporation reactions of the cluster $[\text{Fe}_3\text{S}_4(\text{LS}_3)]^3-$, containing the cuboidal $[\text{Fe}_3\text{S}_4]^0$ core. *J Am Chem Soc* **119**, 6242-6250
30. Moura, J. J. G., Moura, I., Kent, T. A., Lipscomb, J. D., Huynh, B. H., Legall, J., Xavier, A. V., and Munck, E. (1982) Interconversions of [3Fe-3S] and [4Fe-4S] clusters – Mössbauer and electron paramagnetic resonance studies of *Desulfovibrio gigas* ferredoxin-II. *J Biol Chem* **257**, 6259-6267
31. Kent, T. A., Dreyer, J. L., Kennedy, M. C., Huynh, B. H., Emptage, M. H., Beinert, H., and Munck, E. (1982) Mossbauer studies of beef heart aconitase: evidence for facile interconversions of iron-sulfur clusters. *Proc Natl Acad Sci USA* **79**, 1096-1100
32. Robbins, A. H., and Stout, C. D. (1989) Structure of activated aconitase – Formation of the [4Fe-4S] cluster in the crystal. *Proc Natl Acad Sci USA* **86**, 3639-3643
33. Conover, R. C., Park, J. B., Adams, M. W. W., and Johnson, M. K. (1990) Formation and properties of a NiFe₃S₄ cluster in *Pyrococcus furiosus* ferredoxin. *J Am Chem Soc* **112**, 4562-4564
34. Spangler, N. J., Meyers, M. R., Gierke, K. L., Kerby, R. L., Roberts, G. P., and Ludden, P. W. (1998) Substitution of valine for histidine 265 in carbon monoxide dehydrogenase from *Rhodospirillum rubrum* affects activity and spectroscopic states. *J Biol Chem* **273**, 4059-4064
35. Staples, C. R., Heo, J., Spangler, N. J., Kerby, R. L., Roberts, G. P., and Ludden, P. W. (1999) *Rhodospirillum rubrum* CO-Dehydrogenase. Part 1. Spectroscopic Studies of CODH Variant C531A Indicate the Presence of a Binuclear [FeNi] Cluster. *J Am Chem Soc* **121**, 11034-11044

36. Jeon, W. B., Singer, S. W., Ludden, P. W., and Rubio, L. M. (2005) New insights into the mechanism of nickel insertion into carbon monoxide dehydrogenase: analysis of *Rhodospirillum rubrum* carbon monoxide dehydrogenase variants with substituted ligands to the [Fe₃S₄] portion of the active-site C-cluster. *J Biol Inorg Chem* **10**, 903-912
37. Inoue, T., Takao, K., Yoshida, T., Wada, K., Daifuku, T., Yoneda, Y., Fukuyama, K., and Sako, Y. (2013) Cysteine 295 indirectly affects Ni coordination of carbon monoxide dehydrogenase-II C-cluster. *Biochem Biophys Res Commun* **441**, 13-17
38. Kabsch, W. (2010) XDS. *Acta Crystallogr D Biol Crystallogr* **66**, 125-132
39. Otwinowski, Z., and Minor, W. (1997) Processing of X-ray diffraction data collected in oscillation mode. *Methods Enzymol* **276**, 307-326
40. McCoy, A. J., Grosse-Kunstleve, R. W., Adams, P. D., Winn, M. D., Storoni, L. C., and Read, R. J. (2007) Phaser crystallographic software. *J Appl Crystallogr* **40**, 658-674
41. Adams, P. D., Afonine, P. V., Bunkoczi, G., Chen, V. B., Davis, I. W., Echols, N., Headd, J. J., Hung, L. W., Kapral, G. J., Grosse-Kunstleve, R. W., McCoy, A. J., Moriarty, N. W., Oeffner, R., Read, R. J., Richardson, D. C., Richardson, J. S., Terwilliger, T. C., and Zwart, P. H. (2010) PHENIX: a comprehensive Python-based system for macromolecular structure solution. *Acta Crystallogr D Biol Crystallogr* **66**, 213-221
42. Emsley, P., Lohkamp, B., Scott, W. G., and Cowtan, K. (2010) Features and development of Coot. *Acta Crystallogr D Biol Crystallogr* **66**, 486-501
43. Painter, J., and Merritt, E. A. (2006) Optimal description of a protein structure in terms of multiple groups undergoing TLS motion. *Acta Crystallogr D Biol Crystallogr* **62**, 439-450
44. Chen, V. B., Arendall, W. B., 3rd, Headd, J. J., Keedy, D. A., Immormino, R. M., Kapral, G. J., Murray, L. W., Richardson, J. S., and Richardson, D. C. (2010) MolProbity: all-atom structure validation for macromolecular crystallography. *Acta Crystallogr D Biol Crystallogr* **66**, 12-21
45. Schrodinger, LLC. (2015) The PyMOL Molecular Graphics System, Version 1.8.
46. Morin, A., Eisenbraun, B., Key, J., Sanschagrin, P. C., Timony, M. A., Ottaviano, M., and Sliz, P. (2013) Collaboration gets the most out of software. *Elife* **2**

Abbreviations

CODH: carbon monoxide dehydrogenase

S_L: linking sulfide

Fe_u: unique iron

Table 1. Metal content and activity of *Dv*CODH variants

<i>Dv</i> CODH sample	as-isolated Ni/monomer	as-isolated Fe/monomer	as-isolated CO oxidation activity ($\mu\text{mol}\cdot\text{min}^{-1}\cdot\text{mg}^{-1}$)	Ni-reconstituted CO oxidation activity ($\mu\text{mol}\cdot\text{min}^{-1}\cdot\text{mg}^{-1}$)	Ref.
WT ^{+CooC}	0.4–0.9	8–10.5	160	1660	(17)
WT ^{-CooC}	0–0.2	7.5–8.5	<5	4–60	(17)
C301S ^{+CooC}	0	10	N/D	N/D	this work
	0	13	N/D	N/D	(9)
	0	10 \pm 2.5	N/D	N/D	this work
Δ D ^{+CooC}	0.02	8 \pm 1	N/D	<5	this work

Table 2. Crystallographic data collection and refinement statistics

	WT ^{-CooC} as-isolated	WT ^{-CooC} as-isolated Fe peak [†]	WT ^{-CooC} reduced	WT ^{-CooC} reduced Fe peak [†]	(Δ D) ^{+CooC} Fe peak [†]
Data collection					
Wavelength (Å)	0.9792	1.7389	0.9792	1.7389	1.7379
Space group	<i>P</i> ₂₁	<i>P</i> ₂₁	<i>P</i> ₂₁	<i>P</i> ₂₁	<i>C</i> ₂
Cell dimensions					
<i>a</i> , <i>b</i> , <i>c</i> (Å)	64.8, 144.1, 123.4	64.8, 144.2, 123.4	64.7, 143.8, 123.1	64.7, 143.7, 123.2	110.5, 100.6, 65.3
β (°)	98.5	98.5	98.6	98.6	124.7
Resolution (Å)*	100–1.50 (1.53–1.50)	100–1.97 (2.01–1.97)	100–1.72 (1.75–1.72)	100–2.32 (2.37–2.32)	50.0–2.48 (2.57–2.48)
Completeness (%)*	95.0 (93.1)	90.7 (87.3)	95.9 (95.6)	94.2 (93.0)	93.4 (88.6)
Redundancy*	6.5 (6.0)	4.4 (4.3)	5.1 (4.9)	4.3 (4.2)	3.0 (2.0)
Unique reflections*	338890 (24577)	283488 (20224)	225437 (16599)	178944 (13009)	38000 (3637)
<i>R</i> _{sym} (%)*	9.2 (90.4)	12.2 (60.7)	9.3 (91.3)	11.6 (87.5)	22.0 (78.3)
CC _{1/2} *	99.8 (71.2)	99.5 (75.7)	99.8 (68.5)	99.6 (65.0)	95.8 (47.2)
$\langle I / \sigma I \rangle$ *	11.5 (1.9)	7.9 (2.0)	11.3 (2.0)	9.88 (2.1)	6.1 (2.1)
Refinement					
Resolution (Å)	93.3–1.50		93.3–1.72		45.4–2.48
No. reflections	338812		225376		37976
<i>R</i> _{work} / <i>R</i> _{free}	0.154/0.178		0.149/0.176		0.207/0.248
Monomer/asu	4		4		1
No. atoms					
protein	18977		18682		4481
B-cluster	32		32		8
C-cluster	36		36		8
D-cluster	8		8		–
water	2673		1899		25
<i>B</i> -factors					
protein	19.6		22.6		41.5
B-cluster	15.8		16.7		40.3
C-cluster	21.0		24.4		45.6
D-cluster	17.9		18.9		–
water	33.9		34.0		40.7
R.m.s. bond deviations					
Lengths (Å)	0.007		0.007		0.003
Angles (°)	0.932		0.919		0.737
Rotamer outliers (%)	0.15		0.52		0.67

[†]Bijvoet pairs were not merged during data processing.

*Values in parentheses are for the highest-resolution shell.

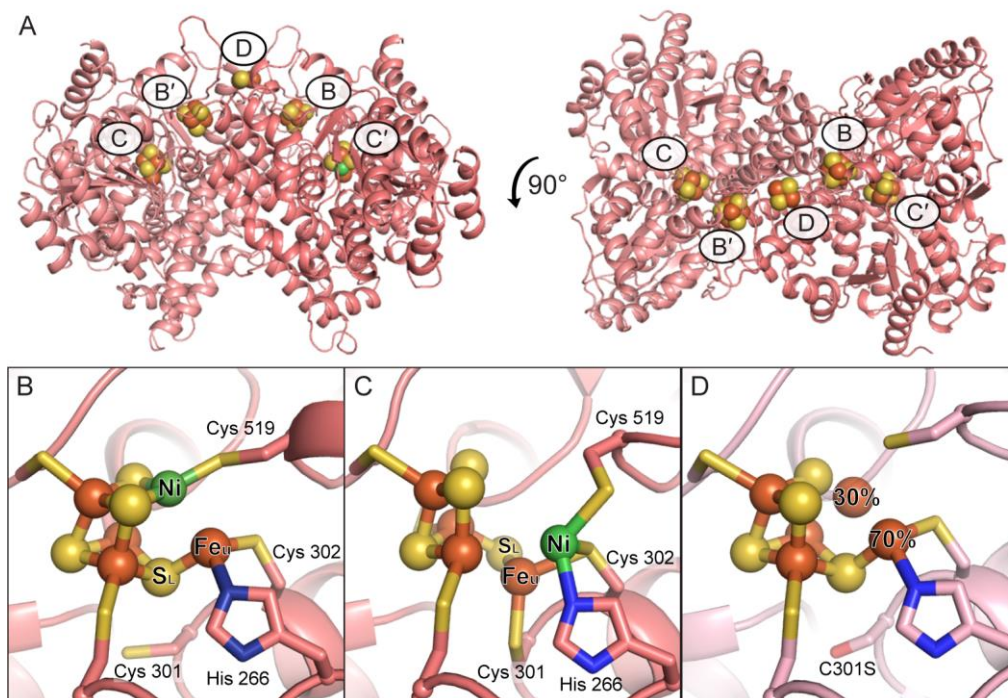


Figure 1. The metalloclusters of CODH. A) The overall homodimeric structure of *Dv*CODH (PDB ID 6B6V). Metalloclusters are shown as spheres and labeled. Note that the B-cluster of one monomer completes the electron transfer pathway of the opposing monomer. B) The C-cluster in its canonical, reduced state (PDB ID 6B6V). C) The oxidized C-cluster (PDB ID 6B6W). A lysine residue that completes a distorted tetrahedral coordination geometry around the Ni ion has been omitted for simplicity. D) The C-cluster of *Dv*CODH(C301S)^{+CooC} (PDB ID 6DC2). Residue numbers correspond to the sequence of *Dv*CODH. Protein is shown in ribbon representation in pink with metalloclusters shown as spheres and sticks with Ni in green, Fe in orange, S in yellow; in panels B–D, ligating amino acid residue side chains are shown as sticks with S in yellow, N in blue, and O in red. Structures shown in this figure are described in Reference (9).

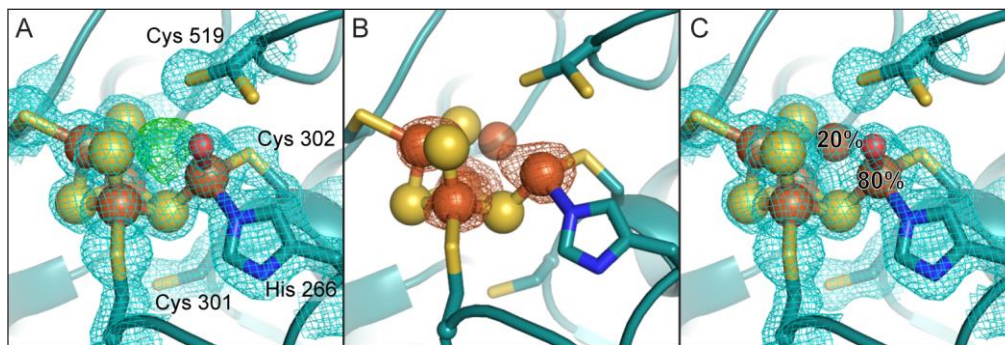


Figure 2. The $DvCODH^{CooC}$ C-cluster is a [3Fe-4S] cluster with a mobile Fe_u . A) Refinement of a [3Fe-4S]- Fe_u C-cluster results in positive F_o-F_c electron density (green mesh, contoured to $+3\sigma$) at the Ni binding site. $2F_o-F_c$ electron density (blue mesh) contoured to 1σ . A water molecule (red sphere) is bound to Fe_u . Cys 519 adopts alternative conformations. B) Fe anomalous difference map (orange mesh, contoured to 6σ) indicates the presence of Fe at partial occupancy in the canonical Ni binding site. The Fe_u -ligating water molecule has been omitted for simplicity. C) The C-cluster refined with an alternative conformation of Fe_u . At 80% occupancy, Fe_u is ligated by His 266 and Cys 302 in its canonical binding site. At 20% occupancy, Fe_u is incorporated into the cubane portion of the cluster and ligated by Cys 519. $2F_o-F_c$ electron density (blue mesh) contoured to 1σ . Protein is shown in ribbon representation in teal with ligating amino acid residue side chains in sticks; cluster ions shown as spheres and sticks; Fe in orange, S in yellow, N in blue, O in red.

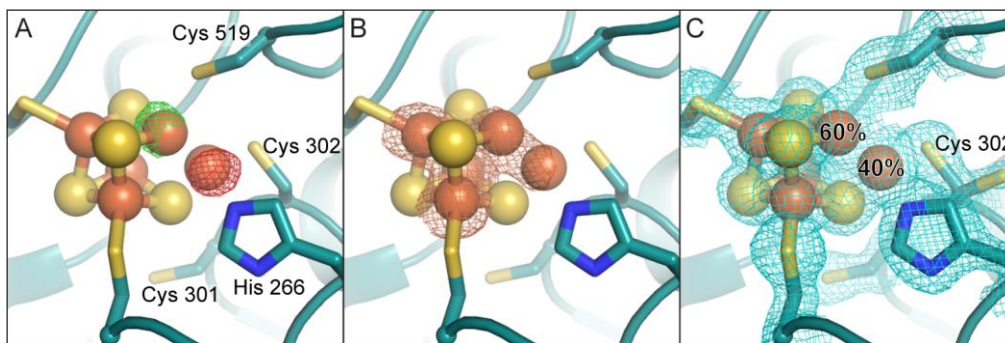


Figure 3. Reduction of $DvCODH^{CooC}$ induces movement of Fe_u into the Fe-S cubane portion of the C-cluster. A) Isomorphous difference map ($F_o(\text{reduced})-F_o(\text{as-isolated})$) reveals increased electron density at the canonical Ni binding site of the cubane (green mesh, contoured to $+5\sigma$) and decreased electron density at the canonical Fe_u binding site (red mesh, contoured to -5σ) in the structure of reduced $DvCODH^{CooC}$ relative to as-isolated $DvCODH^{CooC}$. B) Fe anomalous difference map (orange mesh, contoured to 6σ) reveals a strong peak of Fe anomalous signal in the canonical Ni binding site of the cubane (compare to Figure 2B). C) The C-cluster of $DvCODH^{CooC}$ refined with an alternative conformation of Fe_u . At 60% occupancy, Fe_u is incorporated into the cubane portion of the cluster and ligated by Cys 519. At 40% occupancy, Fe_u is ligated by His 266 and Cys 302 in its canonical binding site. Cys 302 adopts alternative conformations. $2F_o-F_c$ electron density (blue mesh) contoured to 1σ . Protein is shown in ribbon representation in teal with ligating amino acid residue side chains in sticks; cluster ions shown as spheres and sticks; Fe in orange, S in yellow, N in blue.

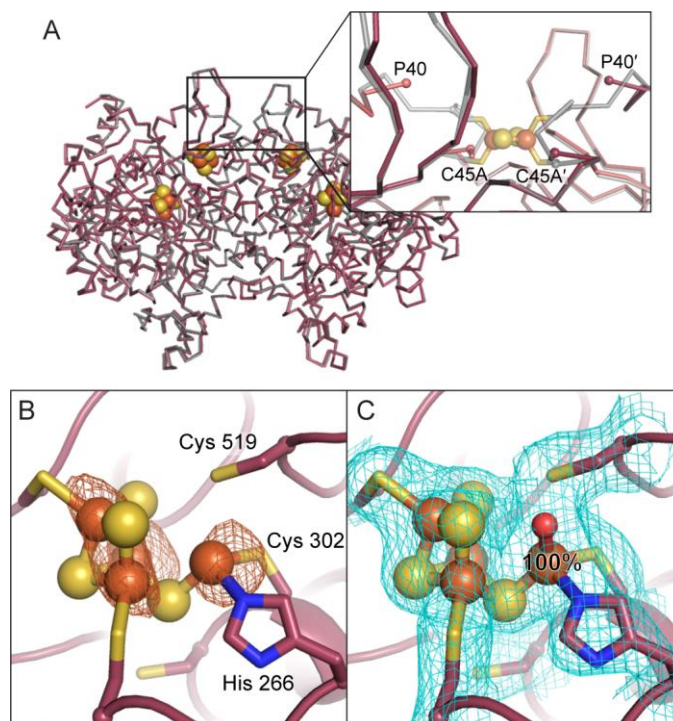


Figure 4. Removal of the D-cluster does not alter the overall structure but leads to incomplete C-cluster assembly. A) Structural alignment of $DvCODH(\Delta D)^{+CooC}$ (maroon) with $DvCODH^{+CooC}$ (grey; PDB ID 6B6V, Ref. (9)). Inset shows disorder in the vicinity of the D-cluster in $DvCODH(\Delta D)^{+CooC}$. Proteins are shown as the $C\alpha$ trace of each structure. B- and C-clusters of $DvCODH(\Delta D)^{+CooC}$ are shown as spheres. B) Fe anomalous difference map (orange mesh, contoured to 5σ) suggests the presence of Fe_u at full occupancy in its canonical binding site. C) Refinement of $DvCODH(\Delta D)^{+CooC}$ confirms the location and occupancy of Fe_u . $2F_o - F_c$ electron density (blue mesh) contoured to 1σ . In panels B and C, protein is shown in ribbon representation in maroon with ligating amino acid residue side chains in sticks; cluster ions shown as spheres and sticks; Fe in orange, S in yellow, N in blue, O in red.

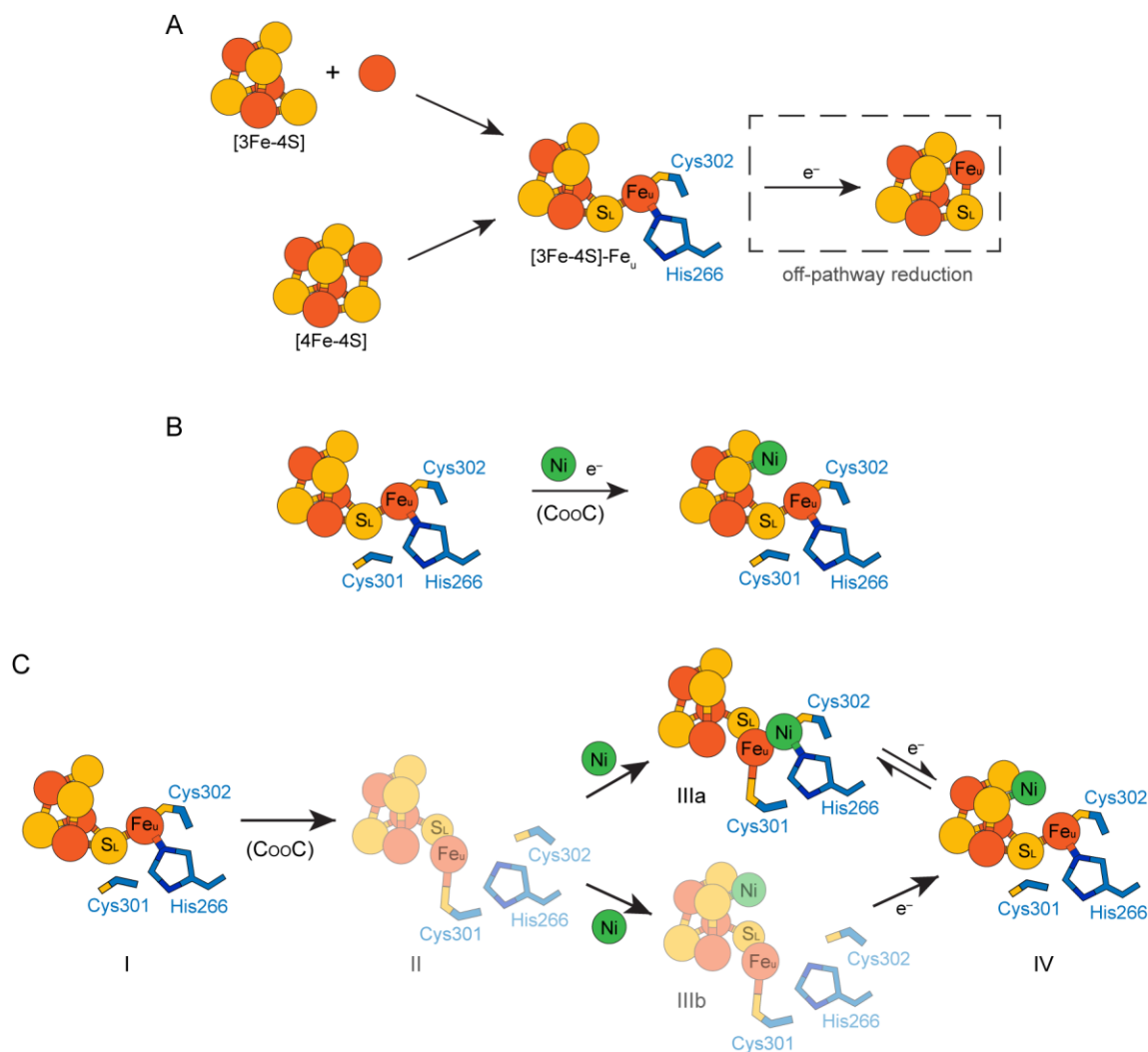


Figure 5. Models of C-cluster assembly. A) Formation of the C-cluster Fe-S scaffold. The Fe-S scaffold could be assembled through two different pathways. First, the components of the C-cluster could be inserted as a [3Fe-4S] cluster that combines with a mononuclear Fe ion (upper pathway). Alternatively, the C-cluster site could become loaded with a [4Fe-4S] cluster followed by removal of an Fe ion from the cubane to form Fe_u (lower pathway). In either case, an off-pathway reduction event could (re)convert the [3Fe-4S]-Fe_u scaffold into a [4Fe-4S] cluster. B/C) Two independent models for nickel insertion into the C-cluster. B) Nickel could be inserted directly into a reduced [3Fe-4S]-Fe_u pre-C-cluster. C) Alternative model for nickel insertion involving multiple C-cluster conformations. Starting from the [3Fe-4S]-Fe_u pre-C-cluster (state I), CooC may be involved in inducing a conformational change in the C-cluster in which Fe_u becomes ligated by Cys 301 (state II). Nickel could then bind in either the canonical Fe_u binding site (as observed in structures of the oxidized C-cluster (9); state IIIa) or in the cubane position (state IIIb). Cluster reduction could then result in formation of the fully mature C-cluster (state IV). Electrons (e⁻) indicate reduction events. In panel C, conformations of the C-cluster that have not been characterized crystallographically are shown in faded colors.